DESIGN OF PHOTON ABSORBERS FOR THE SPring-8-II VACUUM SYSTEM

H. Dewa†, K. Tamura[1], Y. Ueda, S. Takahashi, T. Itoga[1], M. Oishi[1], M. Shoji[1], H. Ota, Y. Taniuchi, M. Masaki, T. Masuda, S. Takano[1], T. Watanabe[1]
Japan Synchrotron Radiation Research Institute (JASRI), Sayo, Hyogo, Japan
[1]also at RIKEN SPring-8 Center (RSC), Sayo, Hyogo, Japan

Abstract

SPring-8-II, the forthcoming fourth-generation light source upgrade of SPring-8, aims to achieve X-ray brilliance approximately two orders of magnitude higher than that of the current facility by reducing the electron beam emittance to 100 pm·rad or less. To fit with the narrow-bore five-bend lattice, the vacuum system features discrete photon absorbers with dedicated pumps along with compact thin-walled stainless steel chambers. Two types of absorbers were developed: a horizontal-insertion type capable of handling a maximum total power of 2.25 kW, and a vertical-insertion type designed for a maximum peak power density of 224 W/mm². The absorber design incorporates a grazing incidence angle on the incident surface to reduce power density, a shielding structure designed to confine scattered radiation, and a flange integrated without brazing or welding to eliminate the risk of vacuum leaks. Copper-chromium-zirconium (CuCrZr) was chosen as the material for its superior thermal conductivity and high yield strength. Finite-element analysis using ANSYS was employed to optimize the cooling-channel layout and to ensure compliance with maximum allowable temperature and stress limits.

INTRODUCTION

SPring-8 is Japan's flagship third-generation synchrotron radiation source that commenced user operation in October 1997. Its upgrade, SPring-8-II, has three primary objectives: enhancing light source performance, refurbishing aging systems, and reducing overall power consumption [1]. To achieve an increase of approximately two orders of magnitude in X-ray brilliance compared to the current facility, SPring-8-II targets an ultra-low emittance of 100 pm·rad or less by employing a five-bend lattice comprising densely packed high-gradient magnets, which necessitates reduced vacuum chamber apertures.

To protect these narrow chambers from bending magnet radiation, discrete photon absorbers with grazing-incidence surfaces are deployed to manage the high incident power density. These absorbers utilize materials with high thermal conductivity and resilience to thermal stress, supplemented by water cooling to maintain temperatures within operational limits. This paper presents the design of SPring-8-II photon absorbers validated through thermal-structural analysis.

†dewa@spring8.or.jp

DESIGN OF PHOTON ABSORBERS

The five-bend lattice was designed to reuse the existing tunnel and beamline layout, maintaining the same 48-cell configuration as SPring-8. Within these spatial constraints [2], a total of 14 absorbers are installed per cell [3] to protect the compact vacuum chambers from synchrotron radiation. Table 1 summarizes the total radiation power and peak power density for each absorber. Embedded (Emb) types are integrated into the bending section chambers, whereas discrete horizontal (Hor) and vertical (Ver) insertion absorbers are installed between vacuum chambers. Because the Emb types are subjected to sufficiently low radiation power and power density, they present no significant thermal design issues. The two discrete types are selected based on radiation power and installation constraints. High-power absorbers, as significant sources of photo-stimulated desorption (PSD) gas, are evacuated using an integrated pumping system consisting of a non-evaporable getter pump and a sputter ion pump [3].

Table 1: Total Power and Peak Power Density of the Radiation at the Absorbers for SPring-8-II

Absorber	**IDD**	**AB1**	**AB2**	**CR1**	**BCA2**	**AB3**
Power [kW]	0.67	0.029	1.30	0.22	0.22	0.88
Power density [W/mm2]	17.5	13.5	99.2	27.8	11.6	224
Type	Hor	Hor	Hor	Hor	Emb	Ver

AB4	**AB5**	**AB6**	**AB7**	**CR2**	**AB8**	**BCAS**	**AB9**
0.99	0.85	1.98	1.18	2.25	0.31	0.28	0.68
185	28.4	182	40.4	164	38.7	13.0	129
Ver	Hor	Hor	Hor	Hor	Ver	Emb	Hor

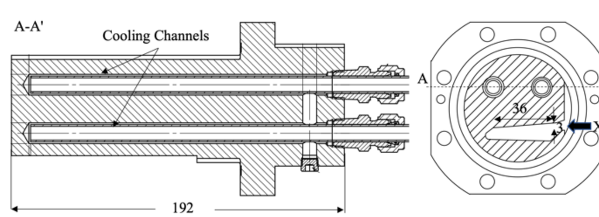

Figure 1: Schematic views of the horizontal-insertion absorber. The cross section (left) is cut along A-A' in the right view.

Among the horizontal-insertion absorbers, AB6 exhibits the highest power density at 182 W/mm², while CR2 receives the highest total power of 2.25 kW. As shown in Fig. 1 (right), the shape is cylindrical, and the incident surface is inclined at a grazing angle of 4.76° to reduce the surface power density. Furthermore, the lower part of the radiation entrance is tapered into a jaw-like shape to prevent scattered X-rays from escaping back through the opening.

Figure 2 shows the absorbed power distribution calculated using the particle transport code PHITS [4]. The simulation assumed a uniform incident X-ray beam, approximating the irradiation of AB6. The plotted values represent the total power integrated horizontally (x) with a y × z mesh resolution of 1 mm × 1 mm. The results indicate that approximately 1/20 of the incident radiation power is deposited on the lower surface, while the power escaping the absorber is suppressed to 1/80 of the initial value. This design confines the majority of scattered radiation within the shield while simultaneously localizing PSD outgassing. This shielding structure mitigates radiation damage to peripheral components, enhancing the vacuum system's long-term robustness and reliability.

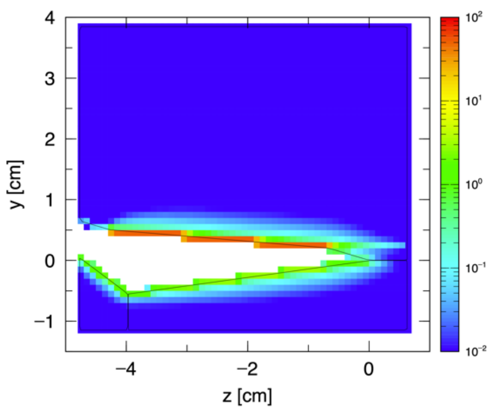

Figure 2: Absorbed power distribution calculated using the PHITS code (see text).

CuCrZr alloy was selected for the absorbers due to its high thermal conductivity and excellent heat resistance. GlidCop was excluded from this application due to cost and availability considerations. To avoid vacuum leaks at dissimilar metal joints and strength degradation from joining heat, the flange and absorber body were monolithically machined from a single block of CuCrZr alloy. This structure is sealed to the vacuum chamber using a metal O-ring.

To suppress the temperature rise caused by the high heat load of synchrotron radiation, the interior of the absorber is water-cooled via two sets of coaxial cooling channels. Inducing turbulent flow at their tips significantly enhances heat transfer efficiency. Each assembly consists of an outer channel (12mm inner diameter) and an inner tube (10mm outer diameter and 8 mm inner diameter).

In contrast, vertical-insertion absorbers are utilized in locations where the horizontal-insertion type cannot be used due to interference with the photon extraction ducts. The power density on AB3 is the highest among all absorbers, but the heat load remains moderate. Figure 3 shows schematic views of the vertical-insertion absorber. Similar to the horizontal type, the absorber features a monolithic structure made of CuCrZr. Although the overall body of the vertical absorber is rectangular, the geometry of the incident surface—including the inclination angle—is identical to that of the horizontal-insertion type.

Unlike the horizontal-insertion type, where the cooling channels run parallel to the incident surface, the channels in the vertical type are oriented vertically. Although this orientation is less efficient for heat transfer, the cooling performance is maintained by doubling the number of channels to four. This configuration enables intensive cooling near the surface, making it effective for high-power-density applications such as AB3. In the special cells upstream and downstream of the beam injection section, the vertical-insertion type is also adopted for absorbers in high-power-density areas, even in locations free from interference with photon extraction ducts. On the other hand, the requirement for four cooling circuits precludes the threaded internal pipe mounting used in the horizontal-insertion type, necessitating electron beam welding (EBW).

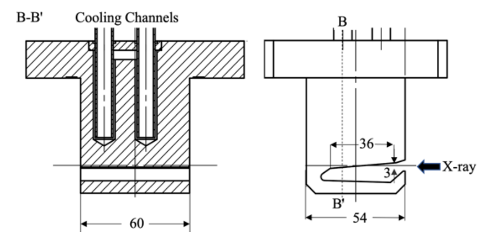

Figure 3: Schematic views of the vertical-insertion absorber. The cross section (left) is cut along B-B' in the right view.

NUMERICAL SIMULATION

The absorber design must prevent surface cracking and cooling water boiling. To ensure this, thermal-stress simulations were conducted using ANSYS [5], a finite element method code. First, the synchrotron radiation heat loads were calculated using a radiation calculation code SPECTRA [6]. These loads were then applied to 3D models of three key absorber types—AB3, AB6, and CR2—to evaluate their temperature and stress distributions. Furthermore, cooling channel positions were optimized through these calculations. Table 2 summarizes the physical properties of CuCrZr used in the simulations, which were determined primarily based on the values reported in previous studies [7, 8].

Table 2: Used Properties of CuCrZr

Thermal conductivity [W/m/K]	318.2
Young's modulus [GPa]	128
Coefficient of Thermal Expansion [10^{-6}/K]	17.5
Density [g/cm^3]	8.89
Specific heat [J/kg/K]	385
Poisson's ratio	0.3

The synchrotron radiation beam position is subject to deviations caused by hardware malfunctions or other operational issues. To ensure safety, we calculated the spatial shifts of the radiation at the absorber positions corresponding to the electron beam's interlock thresholds. Unlike horizontal deviations, vertical shifts can cause a substantial temperature rise. Therefore, simulations were performed for three scenarios—the nominal position, upper limit, and lower limit—to assess the resulting temperature rise.

Although higher flow rates enhance cooling performance, they also increase the risk of erosion. Thermal-stress analyses were performed to identify the minimum flow rate required for effective cooling. The heat transfer coefficients for flow rates of 3, 4, and 5 L/min were set at 6982, 8536, and 10000 W/m²K, respectively, with locally increased values of 8471, 9571, and 10000 W/m²K at the channel tips to account for impingement and turbulence. The cooling water temperature was assumed to be 30 °C. Based on CuCrZr properties at 300 °C [7, 8], the design criteria were defined as follows: a peak surface temperature below 300 °C and an equivalent stress within 250 MPa. Furthermore, the cooling wall temperature was limited to 133 °C, corresponding to the boiling point of water at a gauge pressure of 0.2 MPa.

Worst-case simulation results for AB3, AB6, and CR2 are summarized in Table 3, with (U) representing the upper limit case and (L) the lower limit case. For the AB3 vertical-insertion model, despite having the highest power density among all absorber models, a flow rate of 3.0 L/min maintains the peak surface temperature at 188 °C and the peak cooling wall temperature at 81.1 °C. The equivalent stress at the incident point is approximately 100 MPa. Due to the low heat load, these values remain well within the design criteria even at this flow rate.

In contrast, the horizontal-insertion model for AB6 exhibits a significant temperature rise due to its high radiation power density, reaching 300 °C at a flow rate of 3.0 L/min. While the equivalent stress of 227 MPa provides an adequate safety margin, the cooling channel wall temperature exceeds the 133 °C limit at flow rates of 3 and 4 L/min. Consequently, a flow rate of 5.0 L/min is required to keep the wall temperature below 133 °C.

For the CR2 horizontal-insertion model, the total power is the highest among all types, but the power density is lower than that of AB6. Even at 3.0 L/min, the temperature remains low with a moderate equivalent stress of 192 MPa, which allows for stable operation at this flow rate. Overall, thermal-stress analyses confirmed that AB3 and CR2 operate safely at 3.0 L/min, whereas AB6 requires 5.0 L/min for safe operation.

Table 3: Worst-Case Simulation Results

Absorber (Type)	Water Flow Rate [L/min]	Incident Surface Temperature [°C]	Cooling Channel Temperature [°C]	Equivalent Stress [MPa]
AB3 (Ver)	3	188 (U)	81.1 (U)	100 (L)
	4	184 (U)	77.0 (U)	100 (L)
	5	182 (U)	74.3 (U)	100 (L)
AB6 (Hor)	3	300 (U)	146 (U)	227 (L)
	4	290 (U)	135 (U)	227 (L)
	5	284 (U)	128 (U)	227 (L)
CR2 (Hor)	3	214 (U)	110 (U)	192 (L)
	4	206 (U)	101 (U)	193 (L)
	5	202 (U)	96 (U)	192 (L)

To verify the material parameters used in these calculations, we measured the physical properties of CuCrZr alloys sourced from two domestic suppliers (Samples A and B). The results are summarized in Table 4. Both samples demonstrated excellent thermal and mechanical properties. Specifically, Sample B showed superior yield strength, further enhancing the design reliability. Based on these comprehensive results, both materials satisfy the safety requirements; consequently, Sample B was selected for fabrication, primarily due to economic considerations.

Table 4: Measured Properties of CuCrZr

	Sample A	Sample B
Thermal conductivity [W/m/K] @325°C	362-364	365-368
Young's modulus [GPa] @325 °C	120-121	118-122
Coeff. of Thermal Expansion [10^{-6}/K]	17.9	17.9
Density[g/cm^3] @Room Temp	8.89~8.90	8.90~8.91
Specific heat[J/kg/K] @325 °C	437~440	417-425
Poisson's ratio @Room Temp	0.33-0.34	0.29-0.30
Yield Strength [MPa] @300 °C	258-296	294-324
Tensile Strength [MPa] @300 °C	323-340	325-352

FABRICATION OF THE ABSORBERS

Each CuCrZr absorber body, with an integrated flange, is machined from a monolithic solid block as shown in Fig. 4. The coaxial cooling channels are subsequently assembled by inserting 10-mm-diameter tubes into the body. To prevent vibration and ensure concentric alignment, three 1-mm-diameter rods are TIG-welded onto the outer surface of the inner tube as spacers. For horizontal-insertion absorbers, four notches are machined at the tip of the inner tube to facilitate water circulation. For vertical-insertion absorbers, four cooling channels are precisely aligned with 1-mm spacing and then secured via EBW.

Fabrication of the absorbers is currently underway, and the initial sets have already been completed. No issues have been encountered during machining, and vacuum integrity has been confirmed for all units produced to date.

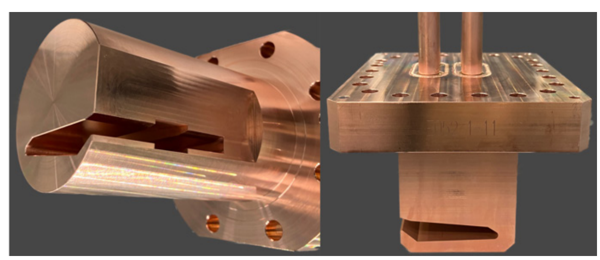

Figure 4: Photographs of the horizontal-insertion absorber (left) and the vertical-insertion absorber (right).

SUMMARY

We have developed photon absorbers specifically designed for the SPring-8-II upgrade. To withstand the high total power and peak power density of bending magnet radiation, a grazing-incidence geometry and CuCrZr alloy were adopted. By incorporating a monolithic design with an integrated flange structure, we eliminated joints between dissimilar metals, thereby enhancing the overall structural reliability. Thermal-stress analyses confirmed that temperature and stress levels remain within the established design criteria. Fabrication of the initial sets of absorbers has been successfully completed.

REFERENCES

[1] H. Tanaka *et al.*, "Green upgrading of SPring-8 to produce stable, ultrabrilliant X-ray beams", *J. Synchrotron Radiat.*, vol. 31, no. 6, pp.1420-1437, Nov. 2024. doi.org/10.1107/S1600577524008348

[2] K. Tanura *et al.*, "Verification of SPring-8-II Vacuum System Prototype Chamber", in *Proc. 13th Int. Conf. Mech. Eng. Des. Synchrotron Radiat. Equip. Instrum. (MEDISI'25)*, Lund, Sweden, Sep.2025, pp. 409-412. doi:10.18429/JACoW-MEDISI2025-THP59

[3] Y. Ueda, *et al.*, "Beam Lifetime Evaluation based on simulation of a Vacuum Pressure Distribution for the SPring-8-II Commissioning Strategy through Vacuum Conditioning", presented at IPAC'26, Deauville, France, May 2026, paper TUP7690, this conference.

[4] T. Sato, *et al.*, "Recent improvements of the Particle and Heavy Ion Transport code System - PHITS version 3.33", *J. Nucl. Sci. Technol.*, vol. 61, pp. 127-135, 2024. doi:10.1080/00223131.2023.2275736

[5] Ansys, `https://www.ansys.com`

[6] T. Tanaka *et al.*, "Major upgrade of the synchrotron radiation calculation code *SPECTRA*," *J. Synchrotron. Radiat.*, vol. 28, pp. 1267-1272, 2021. doi:10.1107/S1600577521004100

[7] E. Gagliardini, *et al.*, "A New Generation OF X-Ray Absorber for the ESRF EBS Storage ring", presented at MEDSI'16, Barcelona, Spain, Sep. 2016, paper TUPE27, unpublished.

[8] Y. Li, *et al.*, "Vacuum joint CuCrZr alloy for high-heat-load photon absorber", *J. Synch. Rad.*, vol. 29, no. 2, pp. 363-368, Mar. 2022. doi:10.1107/S160057752101273X